communications biology

Article

https://doi.org/10.1038/s42003-024-06599-3

Dynamic alternations of three-dimensional chromatin architecture contribute to phenotypic characteristics of breast muscle in chicken

Zhang Wang[1,4], Weihua Tian[1,4], Yulong Guo[1,4], Dandan Wang[1], Yanyan Zhang[1], Yihao Zhi[1], Donghua Li[1,2,3], Wenting Li[1,2,3], Zhuanjian Li[1,2,3], Ruirui Jiang[1,2,3], Ruili Han[1,2,3], Guirong Sun[1,2,3], Guoxi Li[1,2,3], Yadong Tian[1,2,3], Hong Li[1,2,3] ✉, Xiangtao Kang[1,2,3] ✉ & Xiaojun Liu[1,2,3] ✉

Breast muscle growth rate and intramuscular fat (IMF) content show apparent differences between fast-growing broilers and slow-growing indigenous chickens. However, the underlying genetic basis of these phenotypic characteristics remains elusive. In this study, we investigate the dynamic alterations of three-dimensional genome architecture and chromatin accessibility in breast muscle across four key developmental stages from embryo to starter chick in Arbor Acres (AA) broilers and Yufen (YF) indigenous chickens. The limited breed-specifically up-regulated genes (Bup-DEGs) are embedded in breed-specific A compartment, while a majority of the Bup-DEGs involving myogenesis and adipogenesis are regulated by the breed-specific TAD reprogramming. Chromatin loops allow distal accessible regions to interact with myogenic genes, and those loops share an extremely low similarity between chicken with different growth rate. Moreover, AA-specific loop interactions promote the expression of 40 Bup-DEGs, such as *IGF1*, which contributes to myofiber hypertrophy. YF-specific loop interactions or distal accessible regions lead to increased expression of 5 Bup-DEGs, including *PIGO*, *PEMT*, *DHCR7*, *TMEM38B*, and *DHDH*, which contribute to IMF deposition. These results help elucidate the regulation of breast muscle growth and IMF deposition in chickens.

Breast muscle development is directly related to meat production and quality[1]. During myogenesis in the chicken, primary muscle fibers are formed in the early embryo, secondary muscle fibers grow around the scaffold of primary muscle fibers, and the number of muscle fibers is fixed prior to hatching[2]. At post-hatching, muscle growth occurs through the hypertrophy of existing myofibers and is regulated by protein synthesis and metabolism pathways[3]. Intramuscular fat (IMF) content is a crucial indicator of meat quality and refers to the total amount of fat located between muscle fibers and lipid droplets in muscle cells[4]. IMF deposition and myofiber development occur simultaneously during breast muscle development. With the development of secondary muscle fibers, especially during hatching, intramuscular adipocytes begin to secrete lipid droplets[5]. Therefore, a systematic study of breast muscle development could simultaneously determine the biological characteristics of muscle fiber development and IMF deposition.

Muscle growth and IMF deposition are regulated by complex molecular networks at the transcriptional, post-transcriptional, and epigenetic levels[5–8]. It was well documented that chromatin was characterized with high conformation by hierarchical structural units organized into chromatin territories (CTs), compartments, topologically associating domains (TADs), and loops[9]. The whole genome could be split into two spatial compartments, the regions tending to be more accessible were designated as compartment A and those less accessible were designated as compartment B. The A/B compartment switching could influence the accessibility of transcription factors (TFs) or other regulatory proteins to the genomic regions, and consequently, cause the inhibition or activation of gene expression[10,11]. TAD rearrangements might lead to abnormal intergenic interactions and alter gene expression levels[12–18]. The formation of chromatin loops coordinated accessible chromatin to regulate gene expression; chromatin accessibility

[1]College of Animal Science and Technology, Henan Agricultural University, Zhengzhou, 450002, China. [2]Henan Innovative Engineering Research Center of Poultry Germplasm Resource, Zhengzhou, 450002, China. [3]International Joint Research, Laboratory for Poultry Breeding of Henan, Zhengzhou, 450002, China. [4]These authors contributed equally: Zhang Wang, Weihua Tian, Yulong Guo. ✉e-mail: lihong19871202@163.com; xtkang2001@263.net; xjliu2008@hotmail.com

was gained at loop anchors[19]. However, recent studies have showed that specific chromatin loops could also activate gene expression without altering the accessibility of loop anchors[20].

To date, high-throughput chromosome conformation capture (Hi-C) technology has been utilized to analyze the spatial chromatin architecture and identify cellular long-range chromatin interactions in an unbiased and genome-wide fashion. The assay for transposase-accessible chromatin with high-throughput sequencing (ATAC-seq) is a rapid and sensitive method for integrative epigenomic analysis that can determine chromatin accessibility, map genome-wide TF footprints, and nucleosome positions in accessible regions of the genome[21]. Their combination provides an opportunity to facilitate the identification of candidate genes in various biological processes and their regulatory mechanisms at the three-dimensional (3D) genome level. Increasing evidences have showed that aberrant chromatin interactions contribute to the formation of economic traits in livestock and poultry. It was suggested that breed-specific loops were associated with muscle-related traits in swine[22]. Changes in the 3D structure of chromatin could affect myogenesis via activating the expression of important myogenic genes such as *MEF2C* and *DYRK228*[23]. In poultry, studies have focused on the 3D chromatin architecture of red blood cells, the dynamics of chromatin 3D structure during folliculogenesis, conserved and convergently evolved chromosome architectures, and cooperativity in the global reprogramming of chromatin architecture and transcriptome variation[24,25]. Other previous study revealed that TAD boundary sliding was associated with expression levels of *IGF2BP3* and *HMGCR*[26]. However, how dynamic chromatin higher-order structure and chromatin accessibility activate gene expression during chicken breast muscle development remains unknown.

Yufen (YF) chicken is a dual-purpose line and Arbor Acres (AA) chicken is a popular commercial broiler line. The breast muscle growth rate of AA broilers was significantly higher than that of YF chickens, but the IMF content in YF chickens was significantly higher than that in AA broilers (Supplementary Fig. 1). These characteristics make them great models for studying the effects of dynamic chromatin architecture and accessibility on muscle growth and IMF deposition. In this study, we analyzed the 3D genomic architecture, chromatin accessibility and transcriptome expression profiles during key developmental stages of muscle between the above two breeds. Integrated analysis revealed that the dynamic differences in chromatin architecture and its accessibility between the two breeds were associated with phenotypic variants during muscle development.

Results

Overview of the chromosomal contact, chromatin accessibility, and gene expression profiles during breast muscle development in chickens

We collected breast muscle samples from fast-growing AA broilers and slow-growing YF chickens across four developmental stages: embryonic (6-embryonic-old, E6), fetal (18-embryonic-old, E18), neonatal (1-day-old, D1), and starter chick (1-week-old, W1) stages, and performed Hi-C, RNA-seq and ATAC-seq with the same sample at each time point (Fig. 1a). A total of 15.99 billion raw paired-end reads and 9.30 billion valid interaction reads were obtained from the Hi-C library (Supplementary Tables 1-3). The Hi-C contact maps showed canonical chromatin organization, including A/B compartments (100 kb) and TADs (20 kb), with high reproducibility among replicates (Fig. 1b, c; Supplementary Fig. 2a). More than 50.0% of the interactions were within a range of 1 Mbp (Supplementary Fig. 2b) and the frequency of interactions decreased as the linear genomic distance increased (Supplementary Fig. 2c).

Accessible chromatin regions were mapped using ATAC-seq (Supplementary Fig. 3a). Respectively, 419 and 383 million valid reads were obtained from AA and YF chickens with an overall mapping rate of 95.3% (Supplementary Table 4). After peak calling, 341,674 peaks in AA broilers and 397,358 peaks in YF chickens were identified. Peaks were mainly distributed on the distal intergenic region, followed by a gene promoter 3,000 bp upstream of the transcription start site, 5'UTR, and first exon of the gene (Supplementary Fig. 3b, c). The number of peaks in both breeds steadily increased from the embryonic to the neonatal stage, but drastically declined in the starter phase. There was no significant difference in the number of peaks between the two breeds (Supplementary Fig. 3d).

The differentially expressed genes (DEGs) and breed-specifically up-regulated genes (Bup-DEGs) were identified between adjacent stages in both breeds (Supplementary Table 5). Based on 16,929 quantified genes, 436 Bup-DEGs in AA broilers between the embryonic and fetal stages, 322 between the fetal and neonatal stages, and 794 between the neonatal and starter stages were identified. In YF chickens, 520 Bup-DEGs between the embryonic and fetal stages, 424 between the fetal and neonatal stages, and 437 between the neonatal and starter stages were identified (Supplementary Data 1).

Limited effects of breed-specific transcriptional active regions on the expression of Bup-DEGs

The chromosomes in both AA and YF chickens were divided into 1,455 compartments. The A compartment regains contained 61.97 ± 0.58% of the genome, while the B compartment regains contained 38.03 ± 0.58% (Supplementary Data 2). The B compartment was scattered throughout the chromatin in large macrochromosomes (Chr 1-8), but aggregated on the genome in small microchromosomes (Chr 9-34) except for Chr 35, on which the B compartments were discretely distributed (Fig. 2a). A compartment regains showed significantly higher gene density, GC content and expression levels, as well as shorter lengths than that in B compartment regains in both breeds, suggesting that the A compartment regains correlated with open chromatin[27] (Supplementary Fig. 4).

In each development stage, the number of DEGs between two breeds located at the switched compartments generally increased from E6 to W1 (Supplementary Data 1). The GO enrichment analysis showed that the DEGs were significantly enriched cellular response to oxygen-glucose deprivation and termination of RNA polymerase I transcription at the stage of E6, the calcium-independent cell-cell adhesion mediated by plasma membrane cell-adhesion molecules and positively regulated epithelial cell proliferation involved in wound healing at the stage of E18, the axonogenesis at the D1 stage and microtubule depolymerization at the W1 stage between the two breeds (Supplementary Data 2).

Moreover, compartment switching regains constituted the minority parts of the genome during breast muscle development in both breeds (25.39% of the genome in AA broilers, and 26.37% in YF chickens). In most cases, the compartment switching event underwent only one time (BAAA, ABBB, BBAA, AAAB, AABB, BBBA) across the four developmental stages in both breeds (75.67% of the compartment switching events in AA broilers, and 82.04% in YF chickens) (Fig. 2b). Genes in the stable A-to-A compartments or switched B-to-A compartments showed significantly higher expression levels than those in the stable B-to-B compartments or switched A-to-B compartments (Supplementary Fig. 5a). The stable A-to-A compartments and the switched B-to-A compartments were subsequently defined as transcriptionally active regions (TARs). The TARs accounted for ~60% of the genome during the breast muscle development (Fig. 2C). More than 60% of the upregulated DEGs were located in the TARs (Supplementary Data 2) and were significantly enriched in signaling pathways related to the skeletal muscle development in both AA broilers and YF chickens (Supplementary Fig. 5b).

Respectively, breed-specific TAR distributions were observed between adjacent stages, with 1.95% (AA broilers) and 1.67% (YF chickens) of the genome at the embryonic-fetal period; 1.57% (AA broilers) and 2.20% (YF chickens) during the fetal-neonatal period; and 2.02% (AA broilers) and 4.69% (YF chickens) during the neonatal-starter period (Fig. 2c). The breed-specific TARs contained less than 3% of the total number of Bup-DEGs in each adjacent period. The functional enrichment analysis revealed that the Bup-DEGs located in AA-specific TARs were primarily involved in nerve activity related to muscle contractility, including vagus nerve morphogenesis, chemorepulsion of branchiomotor axon (*PLXNA4*), CD24 biosynthetic processes, activation of meiosis involved in egg activation (*PLCB1*), myofibroblast contraction (*EPDR1*), and negative regulation of sodium-dependent phosphate transport (*SFRP4*) (Fig. 2d; Supplementary Fig. 5c,

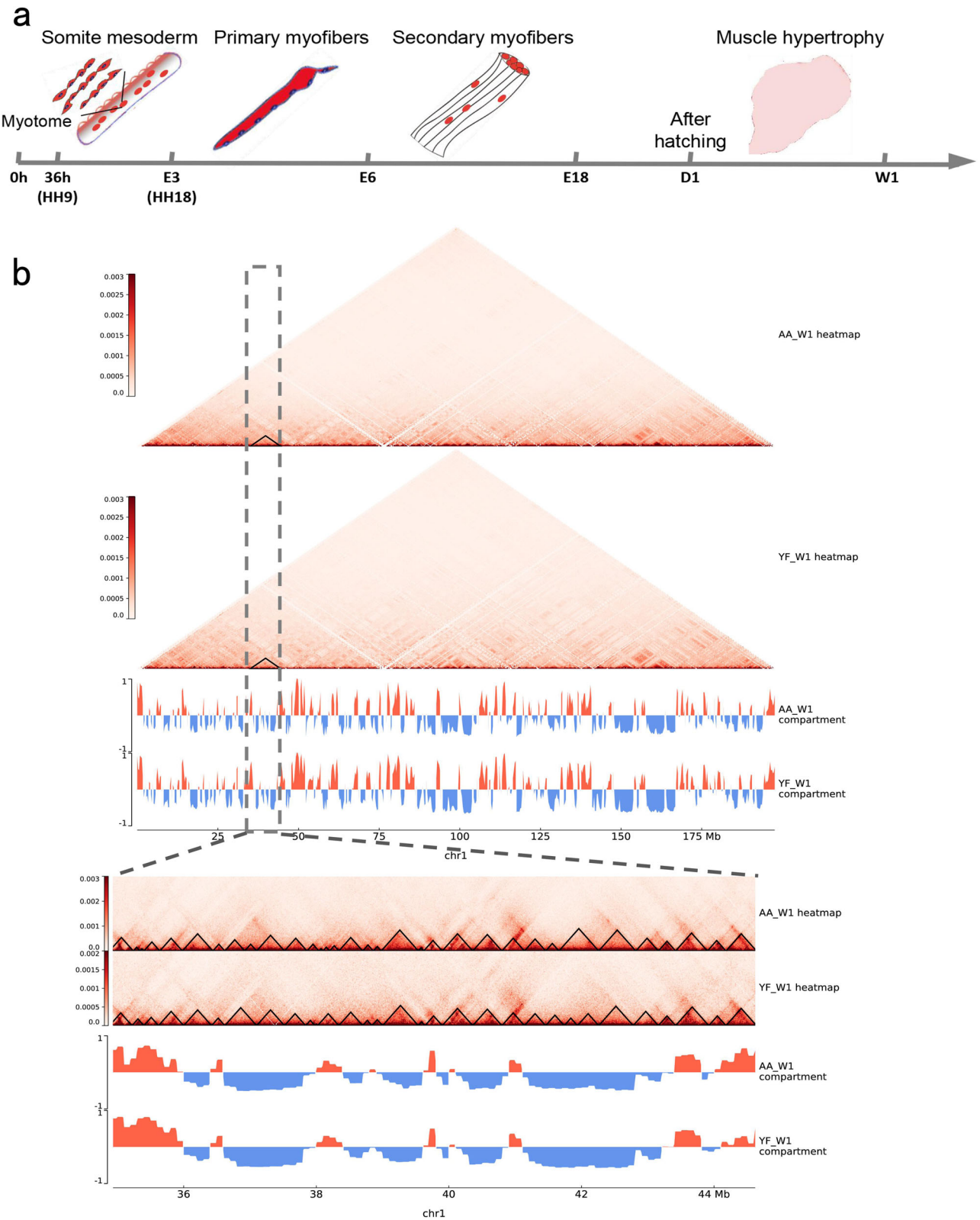

Fig. 1 | Chromosomal contacts during breast muscle development in two chicken breeds. a Developmental characteristics of breast muscle across embryonic, fetal, neonatal, and starter stages in chickens. **b** The canonical chromatin organization, including compartment and TAD, in starter muscles of AA and YF chickens. The top two heatmaps represent chromatin interactions of Chr 1 in AA and YF chickens. The red color from light to dark represents the dynamic changes in chromatin interaction. The next two tracks represent the distribution of chromatin compartments of Chr 1. Positive eigenvalues on the Y-axis represent the A compartment and negative eigenvalues represent the B compartment. The next two heatmaps are the detailed chromatin interaction heatmap of chromosome 1 at 200 kb resolution (Chr 1: 34,934,711-44,620,156). Each equilateral triangle in the local interaction map represents a TAD structure. The lower two tracks represent the distribution of chromatin compartments (Chr 1: 34,934,711-44,620,156). Positive eigenvalues on the Y-axis represent the A compartment and negative eigenvalues represent the B compartment.

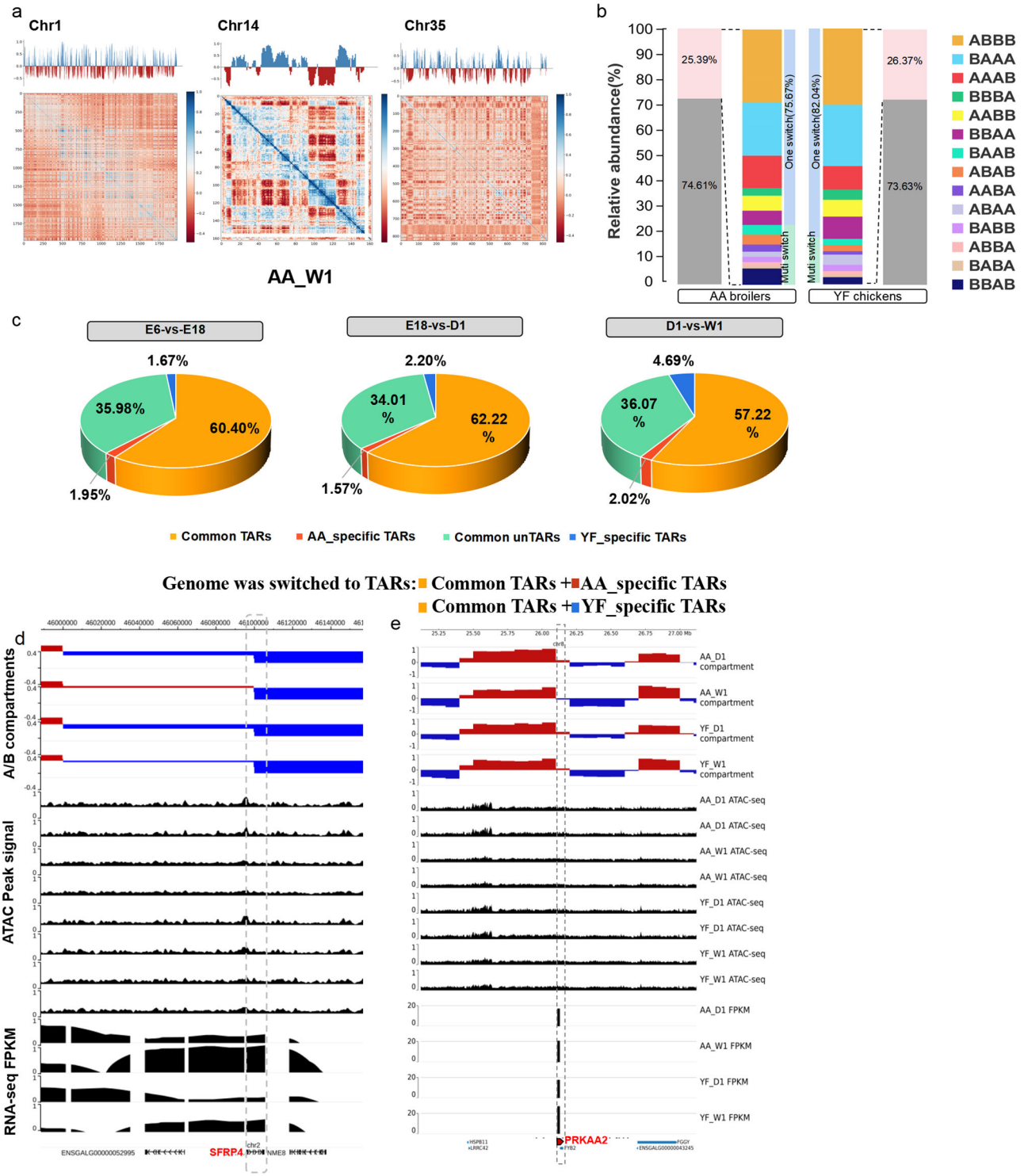

Fig. 2 | Compartmental switching during breast muscle development in two chicken breeds. a The distribution characteristics of the compartments on the linear chromatin. The upper track shows the partitioning of A compartments (blue histogram) and B compartments (red histogram). The lower track shows chromatin interactions in Chr 1, Chr 14, and Chr 35 at 200 kb resolution. **b** The types of switched A/B compartments during muscle development of the two breeds. The outermost grey bars represent stable compartments and the pink bars represent switched compartments. **c** Proportion of chromatin transcriptionally active regions (TARs) in the genome in the breast muscle of adjacent periods. The pie chart divides chromatin into different types based on compartmental switching. The chromatin switched to TARs is the sum of common TARs and breed-specific TARs. **d-e** Two representative functional genes located in TARs during the neonatal and starter stages of two breeds, including *ATAC1* and *SQLE*. The dashed line boxes indicate the chromosomal locations of the interested genes. The tracks show the compartment (top panels), ATAC-seq (middle panels), and gene expression (bottom panels) features at 100 kb resolution.

d, f-g; Supplementary Data 2). Further KEGG analysis showed that the key pathways involved in gap junction, wnt signaling pathway and regulation of actin cytoskeleton (Supplementary Data 2).

The Bup-DEGs located in YF-specific TARs were primarily involved in extracellular matrix growth, muscle atrophy, and immunity, such as heterophilic cell-cell adhesion via plasma membrane cell adhesion molecules (e.g., *NECTIN1*), animal organ development (e.g., *CCDC141*), cellular response to starvation (e.g., *PRKAA2*), arginine catabolic process to glutamate (*OAT*), and extrathymic T cell selection (*IL15*) (Fig. 2e; Supplementary Fig. 5c, e, h-j; Supplementary Data 2). The aforementioned genes are associated with the mTOR signaling pathway, tight junctions, and arginine and proline metabolism. Moreover, the Bup-DEGs at E18 and D1 stages involved in lipid metabolism-related pathways, including adipocytokine signaling pathway (*ACADSB*) and PPAR signaling pathway (*FABP6*) in YF chickens (Supplementary Data 2).

Breed-specific TAD reprogramming was correlated with differences in muscle mass and IMF deposition between the two breeds

At the submegabase scale, we investigated TAD reprogramming during the development of breast muscle in chicken. On average, we identified 3656 TADs in AA broilers and 3616 TADs in YF chickens at 20 kb genomic resolutions, respectively, among which over 50% were distributed in A compartment in both breeds (Supplementary Fig. 6a).

Amounts of the genome displayed TAD reprogramming was induced by TAD boundary sliding or alterations in the intra-TAD interaction frequency of stable TADs between adjacent periods. Of all identified TADs, 32.28 ± 0.83% were boundary sliding and 34.02 ± 0.40% had enhanced or reduced intra-TAD interaction frequencies across both breeds (Fig. 3a; Supplementary Data 3). The boundary-sliding TADs were divided into split, merged, and reorganized types, with merged TADs being the main type (Fig. 3b). In addition, the numbers of stable TADs with enhanced interaction frequency were similar to those with reduced interaction frequency (Supplementary Data 3).

Significantly higher gene density, GC content, and gene expression levels in the TAD boundaries than in the TAD interiors in both breeds (Supplementary Fig. 6b-d). Meanwhile, the expression levels of genes located at stable TADs with enhanced interaction frequency were significantly higher than those with unchanged or reduced interaction frequencies between E6 and E18 stages, D1 and W1 stages in both AA broilers and YF chickens (Fig. 3c, d; Supplementary Data 8). Furthermore, less than half of DEGs at TAD boundary exhibited no sliding (47.24 ± 0.030% in AA broiler and 40.25 ± 0.004% in YF chicken) between adjacent stages. These results suggest that the TAD reprogramming was accompanied by the changes of gene expression. We investigated whether Bup-DEGs were associated with TAD reprogramming during breast muscle development. We identified that 68.73 ± 0.019% of all Bup-DEGs were located either on boundary sliding TADs (35.55 ± 0.015%) or stable TADs with enhanced interaction frequency (33.18 ± 0.033%) between adjacent stages in AA broilers (Supplementary Data 3). GO enrichment analysis revealed that these Bup-DEGs were primarily related to ubiquitin recycling, DNA packaging, negative regulation of immune response, and protein kinase B signaling (Supplementary Fig. 6f). Particularly, during the neonatal and starter stages, Bup-DEGs were significantly enriched in muscle hypertrophy-related GO terms, such as carbohydrate metabolic process, organic acid metabolic process, oxidative phosphorylation, translation, and purine nucleotide metabolic process (Supplementary Data 3). In addition, the significantly enriched pathways of Bup-DEGs included fatty acid degradation, drug metabolism-cytochrome P450, lysine degradation, tyrosine metabolism, tryptophan metabolism, and ubiquitin mediated proteolysis (Fig. 3e, Supplementary Data 3). Fifty-nine of these Bup-DEGs, including *BMP5* and *MRPL16*, were located at stable TADs in both AA broiler and YF chicken, whereas with the enhanced intra-TAD interactions in AA broilers, while the unaltered intra-TAD interactions in YF chickens (Fig. 3f; Supplementary Fig. 6g); 13 of these Bup-DEGs, such as *EIF5B*, were in stable TADs in AA broilers, but in sliding TADs in YF chickens (Supplementary Fig. 6h); while 12 of these Bup-DEGs, such as *SLC2A6*, were in boundary-sliding TADs in AA broilers but in stable TADs in YF chickens (Supplementary Fig. 6j). Additionally, 29 of these Bup-DEGs were located at boundary-sliding TADs and exhibited differential boundary sliding types between the two breeds.

On average, 38.53 ± 0.015% of Bup-DEGs were located in the boundary sliding TADs and 32.35 ± 0.021% were located on stable TADs with enhanced internal interaction strength during adjacent stages in YF chickens (Supplementary Data 3). These genes were primarily enriched in the cellular response to insulin stimulus, sulfur amino acid metabolic processes, chloride ion homeostasis, cellular response to oxygen-containing compounds, and ribose phosphate metabolic processes (Supplementary Fig. 6f). Particularly during the neonatal and starter stages, Bup-DEGs were significantly enriched in lipid metabolism and steroid biosynthesis pathway (Fig. 3e, Supplementary Data 3). Furthermore, several pathways associated with amino acid metabolism, including arginine and proline metabolism, alanine, aspartate and glutamate metabolism, phenylalanine, tyrosine and tryptophan biosynthesis, as well as glycine, serine and threonine metabolism (Supplementary Data 3). And 15 of these Bup-DEGs, such as *DHCR7* and *MFSD2A*, were located in stable TADs and exhibited enhanced intra-TAD interactions in YF chickens, but were unchanged in AA broilers; 4 of these Bup-DEGs, such as *PCYT1A*, were located in stable TADs in YF chickens but in sliding TADs in AA broilers; 5 of these Bup-DEGs, such as *NSDHL*, were located in sliding TADs in YF chickens but in stable TADs in AA broilers. Due to the presence of a sliding boundary, *NSDHL* was located within the intra-TAD region in D1 but positioned at the TAD boundary in W1 of YF chickens. However, *NSDHL* was located within the intra-TAD region at both D1 and W1 in AA broilers, because no TAD sliding events occurred (Fig. 3g, Supplementary Fig. 6k-l). Three of these Bup-DEGs, such as *CERS1* exhibited differential boundary sliding types between the two breeds, with TAD split from the neonatal to the starter stages in AA broilers, with TAD rearrangements in the YF chicken (Supplementary Fig. 6I).

Dynamic alterations in chromatin loops affected breed-specific gene expression during muscle development

More chromatin loops were present during the embryonic and starter stages than the other stages (Supplementary Fig. 7a-d); the number of loops gradually decreased from the embryonic to the neonatal period but suddenly increased in starter across two breeds (Supplementary Fig. 7e). All loops could be divided into three types, including emerging, missing, and unchanged. The similarity rate was used to reflect the proportion of a certain loop type shared by AA broilers and YF chickens to the total number of loops of the corresponding type in an adjacent period. The average values of the similarity rate for adjacent periods were 6.41 ± 3.93% in emerging loops, 10.15 ± 4.88% in missing loops, and 20.18 ± 0.46% in unchanging loops (Fig. 4a; Supplementary Data 4). Regardless of whether it is AA broilers or YF chickens, the expression levels of genes located at emerging loop anchors were significantly higher than those located at missing loop anchors from the embryonic to fetal stages ($p = 0.009$ in AA broilers, $p = 0.002$ in YF chickens), as well as from the neonatal to starter stages ($p < 0.001$ in AA broiler, $p = 0.071$ in YF chicken). Similarly, in comparison to the genes located at missing loop anchors, the genes located at unchanged loops exhibited significantly increased mRNA expression from embryonic to fetal stages in AA broilers ($p = 0.01$) and YF chickens ($p = 0.024$), as well as from the neonatal to starter stages in YF chicken ($p = 0.051$). Nevertheless, there were no difference in the expression of genes located at different loop anchors from the fetal to neonatal stages in both breeds (Fig. 4b, Supplementary Data 9).

Genome-wide accessible regions associated with crucial DNA elements facilitating myofiber growth and IMF deposition

Differential accessibility region (DAR) motif analysis was performed searching for the overrepresentation of TFs binding motifs in the regions of accessible chromatin (Supplementary Fig. 8a; Supplementary Data 5). The most significantly enriched motifs in the AA-gained DARs were Plagl1 during the embryonic period, Hltf during the fetal period, Mzf during the

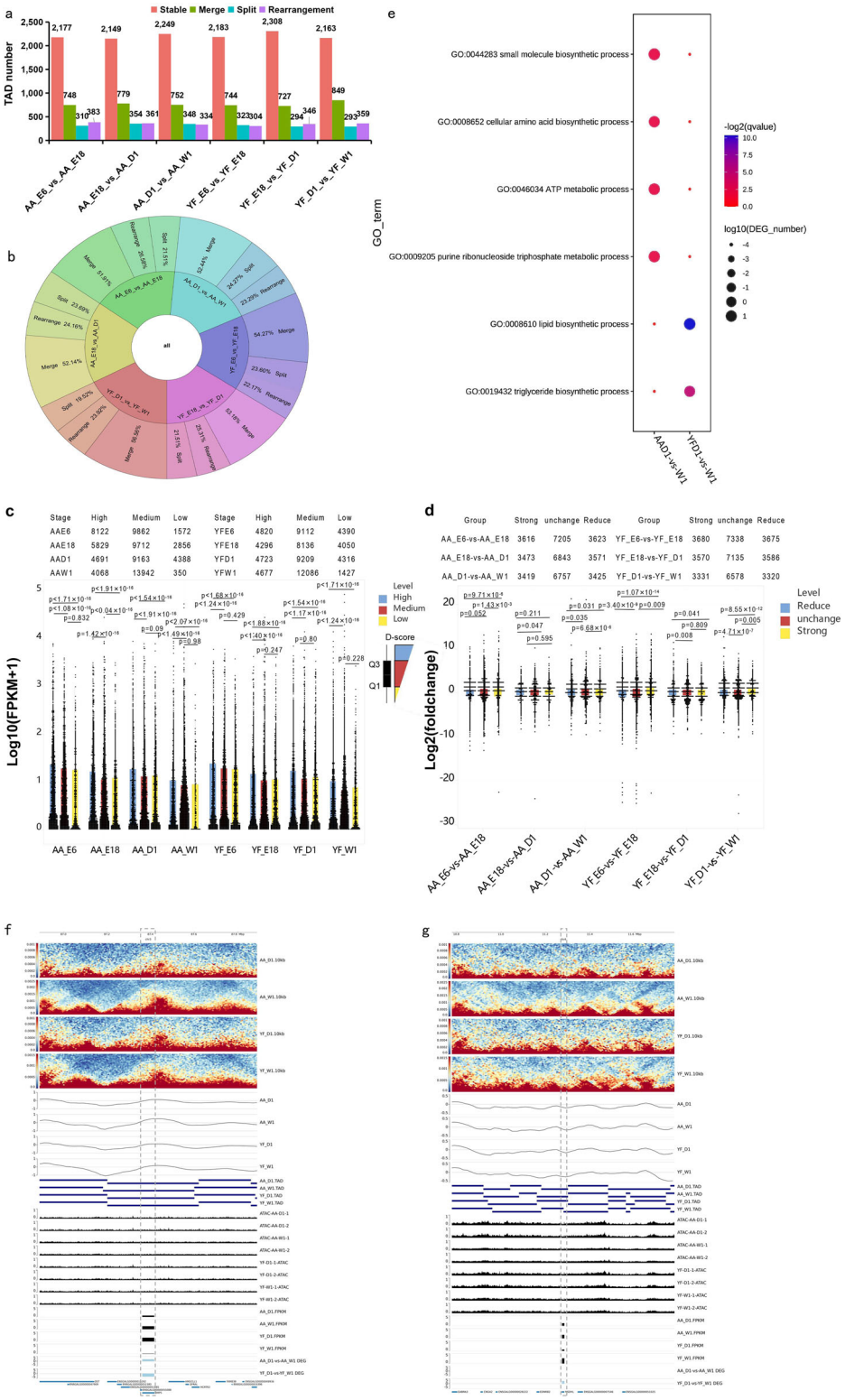

Fig. 3 | Dynamic topologically associating domain features during breast muscle development in AA and YF chickens. a The number of stable topologically associating domains (TADs) and boundary sliding TADs in the comparison of adjacent periods. The sliding events of TADs include merging, splitting, and rearrangement. **b** The proportion of merging, splitting, and rearrangement TAD events to total sliding TADs during breast muscle development of the two breeds. **c** Expression levels of genes located at intra-TADs with a relatively low, medium, or high interaction frequencies during each developmental period. **d** Expression changes in genes with significantly enhanced, decreased, or unchanging interactions between adjacent stages. "Reduce" represented stable TADs with reduced interaction frequencies, "unchange" represented stable TADs with unchanged interaction frequencies, "Strong" represented stable TADs with enhanced interaction frequencies. **e** GO enrichment results of breed-specifically up-regulated genes relative to TADs reprogramming from neonatal to starter stages in AA and YF chickens. **f, g** Two functional genes were subjected to differential interaction frequencies of intra-TAD (*BMP5*) and differential dynamic sliding boundaries (*NSDHL*) during muscle development between two breeds from neonatal to starter stages. The dashed line boxes indicate the chromosomal locations of the interested genes. The top track is Hi-C contact heatmaps of the genomic region around the two functional genes. The tracks in the middle show the dynamic changes of TAD boundaries, ATAC-seq signaling, and gene expression within 20 kb. The TAD was calling by calculating IS with the parameters (−v -is 200,000 -ids 80,000 -im mean -nt 0.1 -bmoe 0) with default parameters at 20-kb resolution. The position of a given TAD in AA broiler chickens corresponds vertically to its position in YF chickens. The boundaries of TAD were represented by equilateral triangles. The stronger the interaction of intra-TAD, the darker the red color inside the triangle. The bottom track displays gene annotations, with the two functional genes shown in red. *P*-values in **c** and **d** were calculated using the two-sided Wilcoxon rank sum test. And the error bars show standard deviation. The exact sample number used for statistics is noted above the box plots. For box plots, the box indicates the first and third quartiles, the line in the box indicates the medians, and whiskers indicate the minimum and maximum data values.

neonatal period, and RARA:RXR during the starter period (Supplementary Fig. 8b; Supplementary Data 5). Among these, PLAGL1 and MZF are extensively documented TFs that facilitate the process of myofiber differentiation and fusion. In YF chickens, the most significantly enriched motifs in gained DARs were FOXL2 during the embryonic period, ZNF148 and KLF4 in the fetal period, RARA:RXR in the neonatal and starter periods, and KLF16 in the starter period (Supplementary Fig. 8b; Supplementary Data 5). Among these, FOXL2 and KLF16 are key TFs that regulate lipid metabolism, whereas ZNF148 inhibits muscle differentiation. The RARA:RXR was significantly enriched in DARs of both breeds, and could interact with myogenesis-related KLF4 and/or adipogenesis-related PPARG, implying its important role in muscle development and IMF deposition.

Gained chromatin accessibility in the promoter region led to a significant increase of gene expression (Fig. 5a). In AA broilers, the promoter regions of 43, 1 and 71 Bup-DEGs exhibited improved accessibility from the embryonic to the fetal stage, the fetal to the neonatal period, and the neonatal

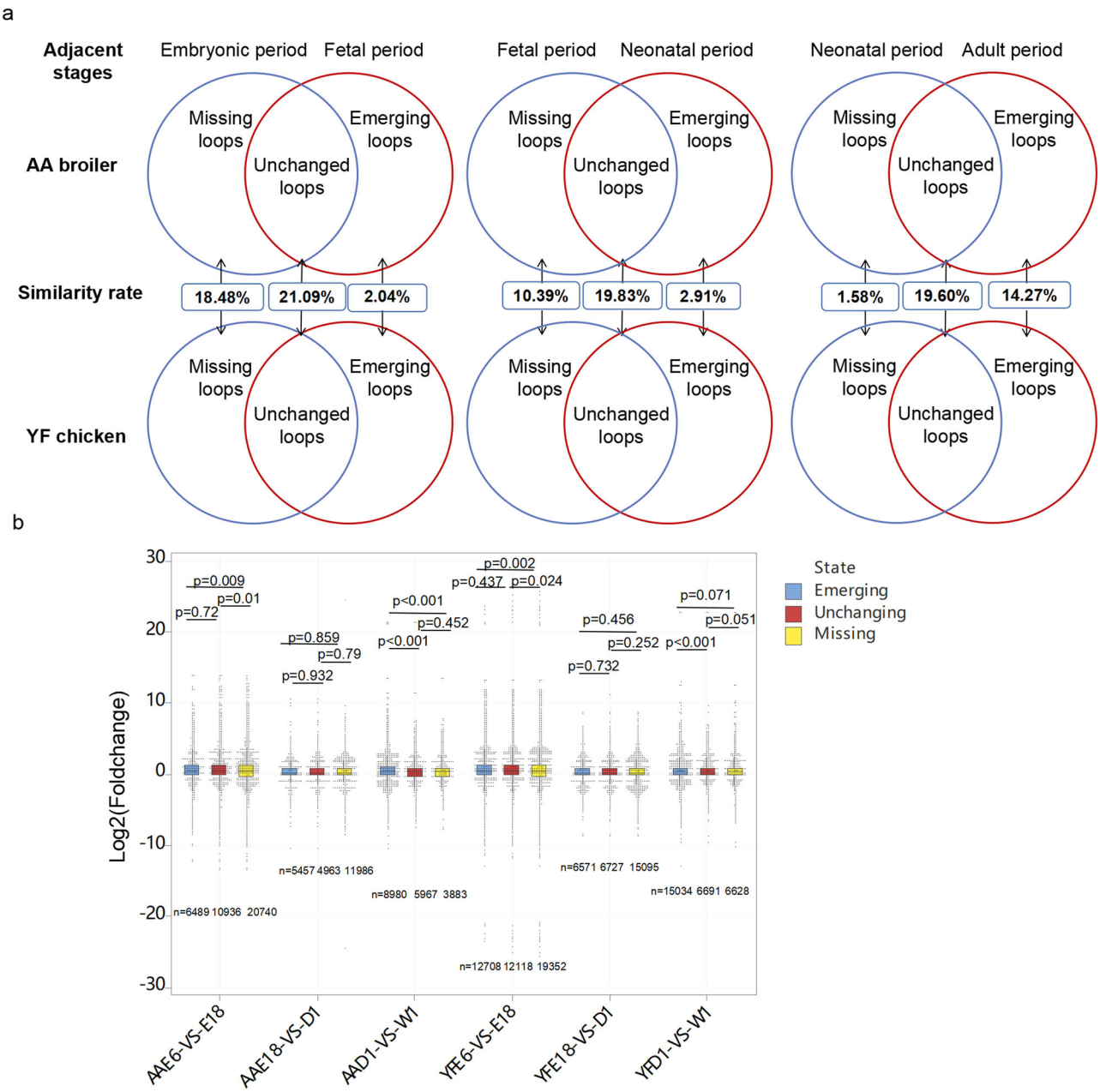

Fig. 4 | Dynamic alteration of chromatin interactions during muscle development in two chicken breeds. a Schematic showing the similarity rate of emerging, missing, and unchanging loops during adjacent periods. The upper tracks shown Venn diagrams of adjacent period loops separating emerging, unchanging, and missing loops in AA broilers, while the lower tracks show the same for YF chickens. The middle track shows the similarity rate of different dynamic type of loops in breast muscle between AA and YF chickens. **b** Changes in the expression of genes located at emerging, missing, or unchanging loop anchors between adjacent periods. *P*-values were calculated using the two-sided Wilcoxon rank sum test. The error bars show standard deviation. For box plots, the box indicates the first and third quartiles, the line in the box indicates the medians, and whiskers indicate the minimum and maximum data values.

period to starter, respectively (Fig. 5b; Supplementary Data 5). The chromatin accessibility in the promoters of *SMTNL1*, *CYCS*, *PLAA* and *FSBP* genes were specifically enhanced, and their mRNA expression was upregulated in breast muscles of AA broilers at the neonatal-starter period (Fig. 5d; Supplementary Fig. S8c-e). In YF chickens, the promoter regions of 101, 14 and 20 Bup-DEGs showed significantly improved accessibility from the embryonic to fetal stage, the fetal to the neonatal stage, and the neonatal to starter stage, respectively (Fig. 5c; Supplementary Data 5). The chromatin accessibility in the promoters of the *HMGCR* gene was specifically enhanced, and its expression was upregulated in breast muscles of YF chickens at the neonatal-starter period (Fig. 5c; Supplementary Data 5).

Breed-specific regulatory mechanisms respond to differences in muscle mass and IMF deposition between the two breeds

Based on the changes in loops and accessibility of loop anchors, the transcriptional regulatory mechanisms of genes were classified into nine patterns (Fig. 6a). Patterns I-III represented emerging loops linked gained, missed and unchanged accessible regions to the target genes, respectively. Patterns IV–VI represented unchanging loops linked gained, missed and unchanged accessible regions to the target genes, respectively. Patterns VII–IX represented changes in accessible promoters when the missing loop could not bring the distal accessible genome and target gene within physical proximity (Fig. 6a). All loop patterns in each category were listed in Supplementary Data 6. Then,

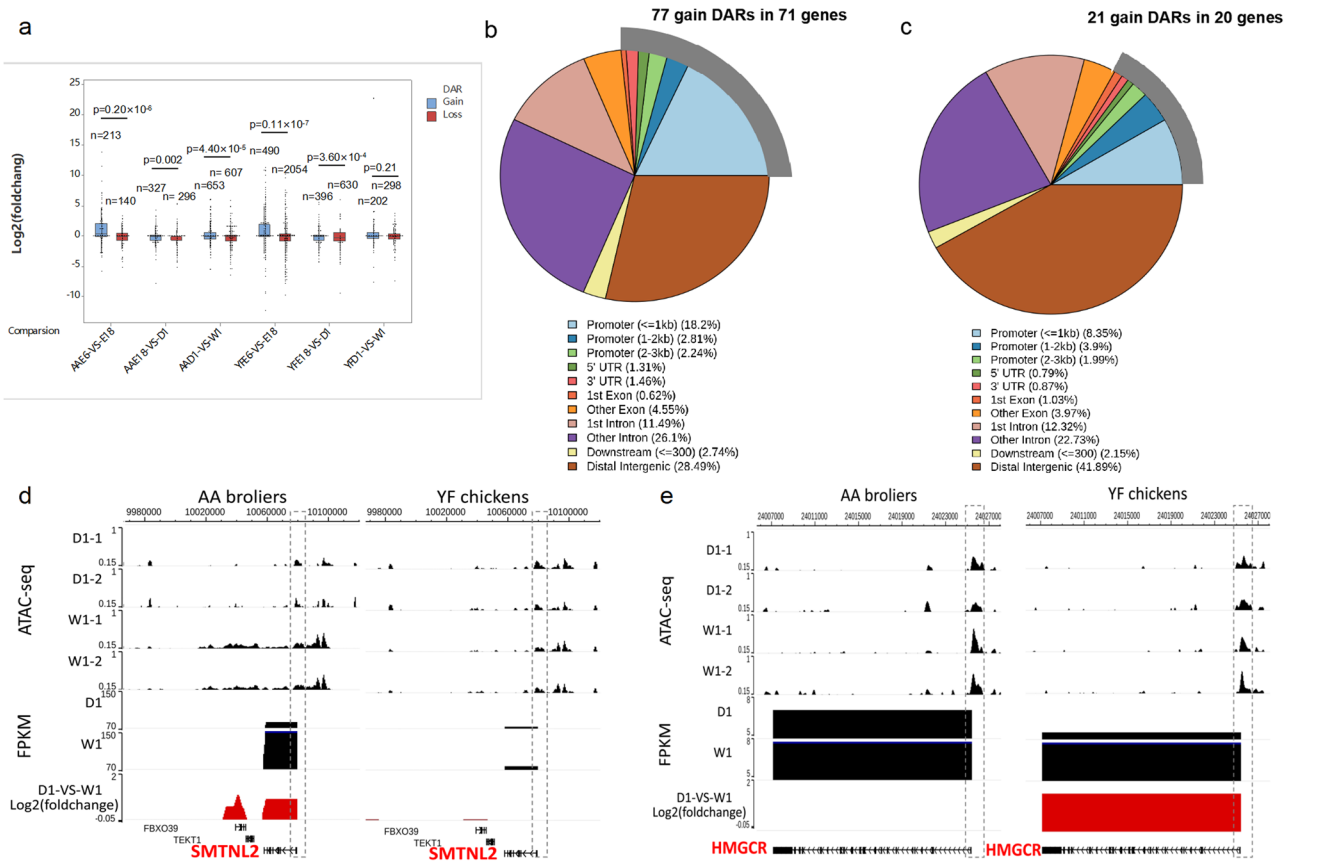

Fig. 5 | The dynamic chromatin accessibility during muscle development of two chicken breeds. a Changes in gene expression when promoter regions are accessible during adjacent periods. **b, c** Genome distribution of differential accessibility regions (DARs) between adjacent periods in AA and YF chickens, respectively. **d, e** Two representative genes, *SMTNL2* and *HMGCR*, showing dynamic alteration of accessibility in the promoter regions during muscle development between the two breeds. The dashed line boxes indicate the chromosomal locations of the interested genes. The top track represents the peak signal, the next track fellow by the gene expression level and the log(foldchange) of the expression level in the comparison of adjacent periods. Gene annotations are shown at the bottom track. *P*-values in **c** were calculated using the two-sided Wilcoxon rank-sum test. The error bars show standard deviation. For box plots, the box indicates the first and third quartiles, the line in the box indicates the medians, and whiskers indicate the minimum and maximum data values.

we analyzed the advantageous patterns regulated gene expression by analyzing the changes in gene expression associated with the 9 patterns across developmental stages in the two breeds. In AA broilers, the genes regulated by the interaction between target gene and distally gained accessible region through emerging loops (pattern I) exhibited enhanced mRNA expression, compared to the genes regulated by the other patterns during the embryonic and fetal stages. The genes exhibited the higher expressions compared with other patterns when the interaction and embedded accessible regions remained unchanged (pattern IV) from fetal to neonatal periods. When the target gene interacted with the distally unchanged accessible region via emerging loops (pattern II), a significant increase in gene expression was observed during the neonatal and starter stages (Fig. 6b; Supplementary Fig. 9a; Supplementary Data 10). In YF chicken, compared to the other patterns, the advantageous patterns that led to significantly increased gene expression were pattern I during the embryonic and fetal stages, patterns I and IV during the neonatal and starter stages, whereas pattern III during the fetal and neonatal stages (Fig. 6b; Supplementary Fig. 9a; Supplementary Data 10). Notably, pattern I not only did not activate gene expression, but also inhibited gene expression during the fetal and neonatal stages (Fig. 6b; Supplementary Fig. 9a; Supplementary Data 10). These results suggest that different developmental stages are supported by different advantageous patterns of activation of gene expression.

Furthermore, we analyzed the biological functions of the Bup-DEGs regulated by the advantageous patterns during adjacent stages. We detected 1, 1 and 179 Bup-DEGs associated with advantageous patterns from the embryonic to the fetal stage, the fetal to the neonatal period, and the neonatal period to starter in AA broilers, respectively (Supplementary Data 7). Particularly during the neonatal and starter stages, 40 Bup-DEGs were significantly enriched in GO terms associated with muscle hypertrophy, namely tRNA aminoacylation, amino acid activation, regulation of amyloid-beta formation, positive regulation of protein polymerization, cortical actin cytoskeleton organization, protein deubiquitination, ubiquitin-dependent protein catabolic processes, and negative regulation of muscle cell apoptotic processes (Supplementary Fig. 9b; Supplementary Data 7). At the same time, numerous pathways related to metabolism, immunity and development were enriched, including aminoacyl-tRNA biosynthesis, ubiquitin mediated proteolysis, TNF, AMPK, p53, IL-17, mTOR, insulin, GnRH and estrogen signaling pathway (Supplementary Data 7). To determine whether these Bup-DEGs were regulated by breed-specific regulatory patterns, we compared the chromatin architecture dynamics in the genomes between the two breeds. In AA broilers, the specific emerging loop linked the distally unchanged accessible regions to the gene promoters (Supplementary Fig. 10a). For example, the emerging loops (chr1: 55100000-55200000, 55200000-55300000) linked the distal unchanged accessible region with the *IGF1* (gene body: chr1:55281078-55330437) from the neonatal to starter stages in AA broilers, thereby significantly increasing its expression, however, no loop-linked distal accessible region for this gene resulted in unchanged expression of *IGF1* in YF chickens (Fig. 6c).

In YF chickens, we detected 40 and 17 Bup-DEGs associated with advantageous patterns from the embryonic to the fetal stage, and the neonatal period to starter, respectively. However, due to the gain-accessible regions or the emerging loops were not the advantageous patterns in the

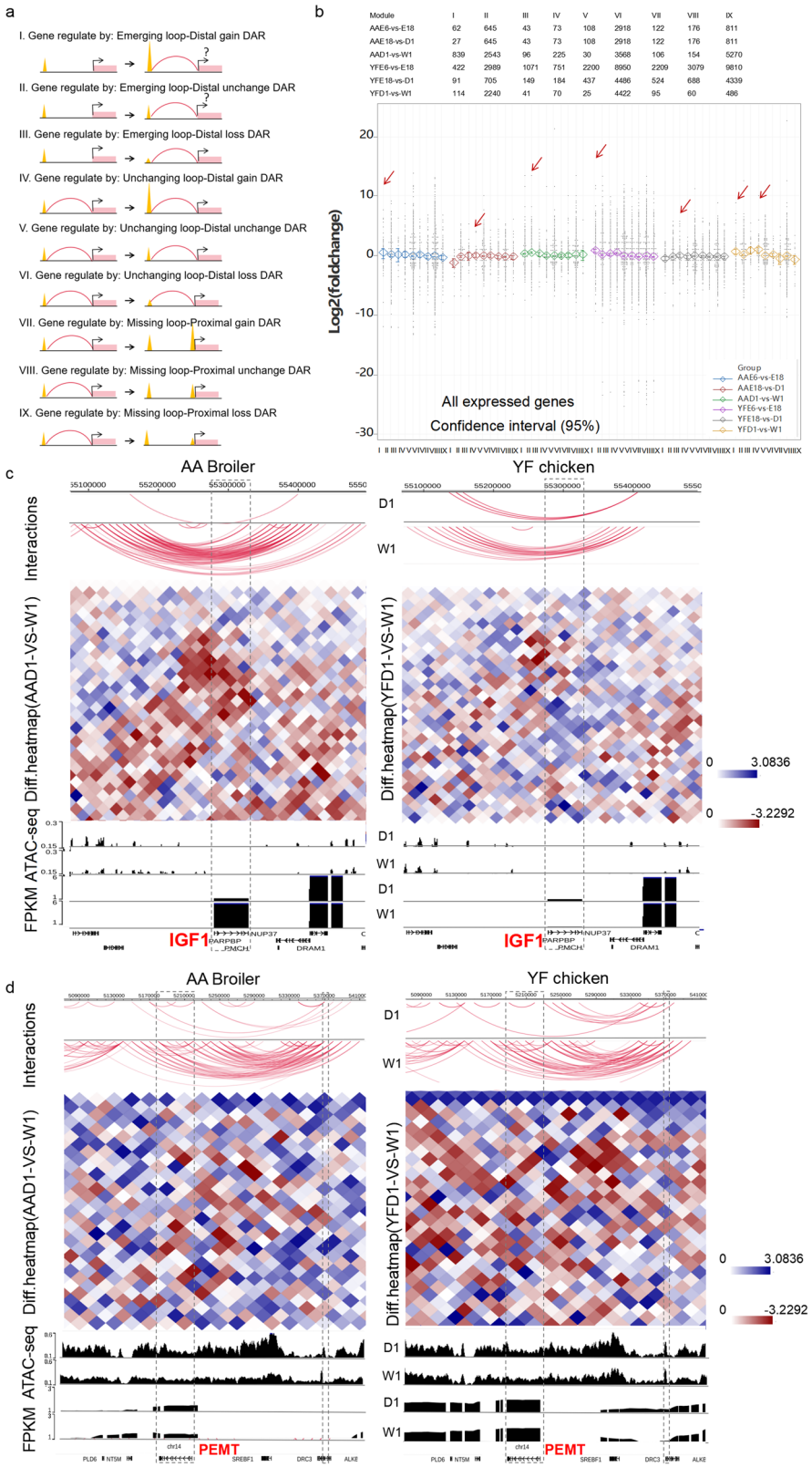

Fig. 6 | Widespread loops link distally accessible regions and promoters to regulate breed-specific transcription. a Nine putative patterns of the 3D genome and their chromatin accessibility for co-activating gene expression. **b** Changes in gene expression associated with each pattern across adjacent periods. **c, d** Epigenetic landscapes of *IGF1* and *PEMT* from the neonatal to starter stages of two chicken breeds. The top track is loop structure mapping genomes around the two functional genes. The next track is the normalized Hi-C contact difference matrix at 10 kb resolution. Red in the heatmap indicates enhanced chromatin interactions in starter muscle and blue indicates enhanced chromatin interactions in neonatal muscle. The lower tracks represent ATAC-seq signal, gene expression, and gene annotation, among which, the two functional genes are marked in red. *P*-values in **b** were calculated using the two-sided Wilcox-on rank sum test and are listed in Supplementary Data 6. The exact sample number used for statistics is noted above the interval plot. The red arrow indicates the regulatory patterns corresponding to the gene with the highest expression level in each group, which also named advantageous pattern in this study. The error bars show standard deviation. For box plots, the box indicates the first and third quartiles, the line in the box indicates the medians, and whiskers indicate the minimum and maximum data values.

fetal and neonatal period, we did not identify the Bup-DEGs associated with advantageous patterns in these stages. During the embryonic and the fetal stage, the Bup-DEGs were primarily involved in sulfur amino acid metabolic processes, regulation of muscle system processes, negative regulation of muscle tissue development, and carbohydrate homeostasis (Supplementary Fig. 9b). The KEGG analysis suggested that these Bup-DEGs were associated with molecular metabolism and signal transduction, such as mucin-type O-glycan biosynthesis, glycine, serine and threonine metabolism, steroid hormone biosynthesis and FoxO signaling pathway (Supplementary Data 7). The Bup-DEG *IGFBP5* was enriched in the negative regulation of skeletal muscle hypertrophy. *IGFBP5* were located within the same TAD in both breeds (Chr7:22670000-23330000) and the intra-TAD interaction

frequency was enhanced from the embryonic to fetal stages in both breeds. There were three contiguous gain-accessible regions (Chr7:22720705-22720895, 22741503-22741772, and 22784934-22785459) distal to *IGFBP5*, which may act as a super-enhancer to activate the expression of *IGFBP5* in YF chickens (Pattern IV). However, because there were no gain-accessible region within this TAD, *IGFBP5* might not link an active enhancer to regulate its expression in AA broilers (Supplementary Fig. 9c).

From the neonatal period to starter in YF chickens, 5 Bup-DEGs (*PIGO*, *PEMT*, *DHCR7*, *TMEM38B*, and *DHDH*) were significantly enriched in phospholipid and lipid biosynthetic processes, steroid biosynthesis, arachidonic acid metabolism and glycerophospholipid metabolism (Supplementary Fig. 9b, Supplementary Data 7). Compared to neonatal stage, a gain-accessible region was linked to the target gene (*TMEM38B*) in starter of YF chickens (Supplementary Fig. 10b). However, the accessibility of this distal region unchanged in AA broilers during the neonatal or starter stages. The other four target genes were linked to the distal gain-accessible region via emerging loops during starter in YF chickens. However, no loops linked the distal gain-accessible region of this gene in AA broilers during the neonatal or starter stages (Fig. 6d, supplementary Fig. 10c).

Discussion

High-quality Hi-C data allowed us to explore the effects of dynamic changes in 3D chromatin architecture on phenotypic differences in the breast muscles of fast- and slow-growing chickens. Our Hi-C datasets revealed a significant disparity in the breast muscle at E6 stage compared to the other stages, which can be attributed to the highest number of E6-specific cis loops. To clarify the difference in dynamically switched compartments between two breeds at the sub-chromosomal level, we defined breed-specific active compartment (A-to-A and B-to-A) as breed-specific TARs during adjacent stages. In actually, breed-specific active compartment (A-to-A and B-to-A) represented the breed-specific TARs, which could active the expression of Bup-DEGs. Furthermore, we identified that chromatin compartmentalization plays an important regulatory role in basic developmental and physiological metabolic processes, such as muscle fiber growth, IMF deposition, and energy and protein metabolism. Although breed-specific TARs contain limited breed-specific genes, the breed-specific expression of these genes may be related to their phenotypic characteristics.

Chicken breast muscle is composed entirely of type IIB glycolytic muscle fibers[28], in which the muscle fibers are larger in diameter in commercial broilers compared with local chickens. Therefore, myosin is hydrolyzed at a faster rate to accommodate quick bursts of contractions[29,30]. In this study, the Bup-DEGs located in the AA-specific TARs regulated neural activity during breast muscle contraction, such as *PLCB1*, *SFRP4*, and *EPDR1*[31]. These results suggest that AA-specific TARs contribute to the high contractile power of broiler breast muscles. It is also known that shorter muscle fiber diameters supply sufficient filling space for the extracellular matrix between cells in slow-growing chickens, which plays an important role in regulating muscle cell proliferation, differentiation, migration, and growth factor activation[29]. We found that the Bup-DEGs located in YF-specific TARs may be related to extracellular matrix growth and muscle atrophy because genes such as *NECTIN1*, *CCDC141*, *PRKAA2*, and *OAT* have been associated with heterophilic cell-cell adhesion via plasma membrane cell adhesion molecules (associated with extracellular matrix growth)[32], animal organ development, cellular response to starvation[33], and arginine catabolic processing to glutamate[34] (associated with muscle atrophy). Moreover, YF-specific TARs could induce the expression of YF-specific up-regulated DEGs associated with lipid metabolism, such as *ACADSB* and *FABP6*, from E18 to D1 in YF chicken. This suggests that these YF-specific TARs promote IMF deposition before hatching in YF chickens, which is consistent with more IMF deposition in YF chickens than in AA broilers. These results suggest that YF-specific TARs may contribute to myofiber diameter, extracellular growth and IMF deposition in slow-growing YF chickens.

TAD reprogramming reflects the changes in local chromatin interactions and can affect gene transcription during myogenesis[35]. In this study, we found that breed-specific TAD reprogramming was associated with Bup-DEGs. Functional enrichment analysis showed that AA-specific up-regulated genes were associated with muscle hypertrophy and quality. As well known, carbohydrate metabolism is one of the most effective ways to increase muscle mass[36]. And oxidative phosphorylation and translation would provide the energy and protein for muscle hypertrophy. The organic acid metabolic process directs our attention to creatine, a crucial organic acid in skeletal muscle that has been proved to stimulate skeletal muscle hypertrophy[37]. In addition, the purine nucleotide metabolic process is responsible for the production of inosine acid, inosine monophosphate (IMP) determined meat quality and help to improve the meat quality of indigenous chicken, which indicate that the lower meat quality might arise from AA-specific TAD reprogramming[38,39]. *BMP5* is a class of cytokines belonging to the TGF-β superfamily and has been implicated in the negative regulation of adipocyte triglyceride synthesis in mammals[40]. *BMP5*-located TADs exhibited enhanced internal interaction frequency in AA broilers but unchanged in YF chickens, leading to the increased expression between D1 and W1 stages. In contrast, some genes upregulated in YF chickens associated with multiple amino acid metabolism and lipid metabolism. These amino acids play diverse physiological functions in muscle growth (leucine, phenylalanine, valine)[41,42] and the biochemical synthesis of creatine (arginine and glycine)[43] to make the meat flavor better[44]. Furthermore, we focused on the YF-specific upregulated DEGs associated with lipid metabolism in YF-specific TADs, which help to clarify the genetic basis of IMF deposition in indigenous chickens, specifically highlighting genes such as *DHCR7*[45] and *MFSD2A*[46], and the internal interaction of these genes-located TADs was enhanced. These results support previous views that TADs limit the physical interactions of transcriptional regulatory elements, such as enhancers and promoters, to construct autonomous gene regulatory regions[47–49]. However, boundary sliding may lead to the deficiency or emergence of enhancer-promoter interaction, subsequently causing complex changes in gene expression[50]. In this study, the percentage of DEGs at stable TAD boundaries was less than that at sliding TAD boundaries, indicating that TAD boundaries sliding was more likely responsible for gene expression regulation. We found some DEGs regulated by boundary sliding were involved in muscle fiber hypertrophy and IMF deposition, including *EIF5B*[51], *SLC2A6*[52], *NSDHL*[53], *PCYT1A*[54], and *CERS1*[55], are located in TADs with sliding boundaries, complicating the interpretation of their transcriptional mechanisms. These results indicate that YF-specific TAD reprogramming played important roles in IMF deposition and skeletal muscle metabolic homeostasis, while AA-specific TAD reprogramming may contribute to muscle mass.

It has been proposed that chromatin loop mediates distal enhancer and thus affect gene transcriptional regulation, and represents a basic unit of chromosome organization because of its fixed anchor position[56]. To gain better knowledge about the contribution of chromatin loops to gene expression regulation during breast muscle development between fast- and slow-growing chicken, we established a similarity rate of chromatin loop to indirectly reflect the differences in chromatin interaction, with the lower similarity rate indicating the greater difference in chromatin 3D conformation. The loop was chosen as the basic unit of analysis because of its fixed anchor position, compared to the sliding boundaries of TADs, and because loops provide more detailed interaction information to identify the differences between breeds. Compared to conserved compartmental switching, the differences in chromatin interactions between breeds were amplified at the loop level. This may be due to the features of the 3D genome structure (from large nuclear compartments and TADs to smaller chromatin loops that connect promoters and enhancers); larger structures are more stable within cells compared to finer structures[57]. Based on dynamic alternations of chromatin loop, we clarified the relationship between chromatin interactions and gene expression. In general, most of chromatin loops showed breed-specific emergence or disappearance during breast

muscle development between the two breeds, and the emergence of loops could elevate the expression of genes on their anchors.

It is well known that the loop-loop interaction is an important transcriptional regulatory mechanism during tissue development[58]. Previous studies suggested that loop anchors maybe overlapped with CTCF signal and enhancer signal (ATAC or H3K27ac) in chicken[24,59,60], which helps us to identify the possible DNA element and related transcriptional mechanism based on the omic datasets in this study. Based on this, we comprehensively examined nine possible patterns of cooperation between chromatin spatial conformation and distally accessible regions in the breast muscle of the two breeds and found that different developmental stages have different advantageous transcriptional regulatory mechanisms. The embryonic and fetal stages are the main periods responsible for myoblast proliferation and differentiation, whereas the neonatal and starter stages are the main periods responsible for muscle fiber hypertrophy[61]. The accessible region interaction was found to be advantageous at these stages, which is consistent with previous studies on myoblasts and adipocytes in mice[35]. However, the fetal and neonatal periods, which are related to neurodevelopment[62], may be more exploration to clarify the advantageous transcriptional regulatory mechanisms. Furthermore, we found that breed-specific interaction changes or distal accessibility changes affected breed-specific gene expression. We found breed-specific loop linking in the distally accessible region to the specifically activates the expression of genes related to muscle hypertrophy in AA broilers, such as *IGF1*[63]. This result elucidate a epigenetic regulatory mechanism that may contribute to muscle fiber over-hypertrophy in AA broilers. In addition, the YF-specific gain-accessible region is linked to the of *IGFBP5* through an unchanging loop, which enhances the YF-specific expression of *IGFBP5* involved in negatively regulated muscle fiber hypertrophy from embryo to fetal stages. Previous studies have shown that muscle fiber hypertrophy is regulated by genes expressed in the muscle at the embryonic or post-hatch stages, even though genetic selection strategies for broilers mainly rely on post-hatch selection[29]. Meantime, we found five YF-specifically upregulated genes (*PIGO*, *PEMT*, *DHCR7*, *TMEM38B*, and *DHDH*) regulated by YF-specific gain-accessible regions or emerging loops related to lipid biosynthesis, and thus affect IMF deposition in YF chickens. These results demonstrate YF-specific EPIs in response to slow-growing muscle growth and IMF deposition in YF chickens. In general, our integrated analysis identified Bup-DEGs regulated by breed-specific loop interactions or accessible regions in response to differences in muscle mass and IMF deposition between the two breeds. However, comprehensively transcriptional mechanisms responsible for these phenotypic diversity need more explore.

Furthermore, genomic variations linked to 3D genomic structure have been observed in animals and plants[22,64,65], which may change the activity or motif function of DNA elements and chromatin interaction. Recent study suggested breed-specific genomic variants regulate the target genes in a long-range manner between fast-growing and slow-growing pig breeds, which suggested that breed-specific variants associated with 3D chromatin architecture between different breeds[22]. Therefore, more genome re-sequencing data is essential to further comprehensively investigated whether genomic variants associated with breed-specific phenotypic characteristics regulated by 3D chromatin architecture. Due to the deficiency of genomic variants in the two chickens breeds in this study, we did not explore the relationship between genomic variations and 3D genomic structure, which needs deeper investigations in our further study.

In conclusion, we examined the dynamic 3D chromatin structures in breast muscle across four key developmental stages from primary and secondary myofibers development and mature to myofibers hypertrophy in fast- and slow-growing chickens. We assess how changes in these characteristics influence the expression of genes related to breed-specific breast muscle characteristics. Our study establish dynamic spatial chromatin architecture maps for breast muscle and demonstrate the contribution of dynamic alterations in genome compartments, topologically associating domains, and widespread chromatin interactions to the phenotypic divergence of breast muscle between fast- and slow-growing chickens (Fig. 7). This study construct a dynamic chromatin architecture of breast muscle and provides insights into the transcriptional regulatory mechanisms of breast muscle growth and IMF deposition in chickens. Our comprehensive genomic data would be helpful for understanding the regulatory mechanisms of muscle development and IMF deposition, and establishing breeding strategy in poultry.

Methods

Ethics statement

This study was approved by the Animal Care Committee of Henan Agricultural University (Zhengzhou, China). Handling procedures were performed in accordance with the standards set by the committee (approval number 11-0085). We have complied with all relevant ethical regulations for animal use.

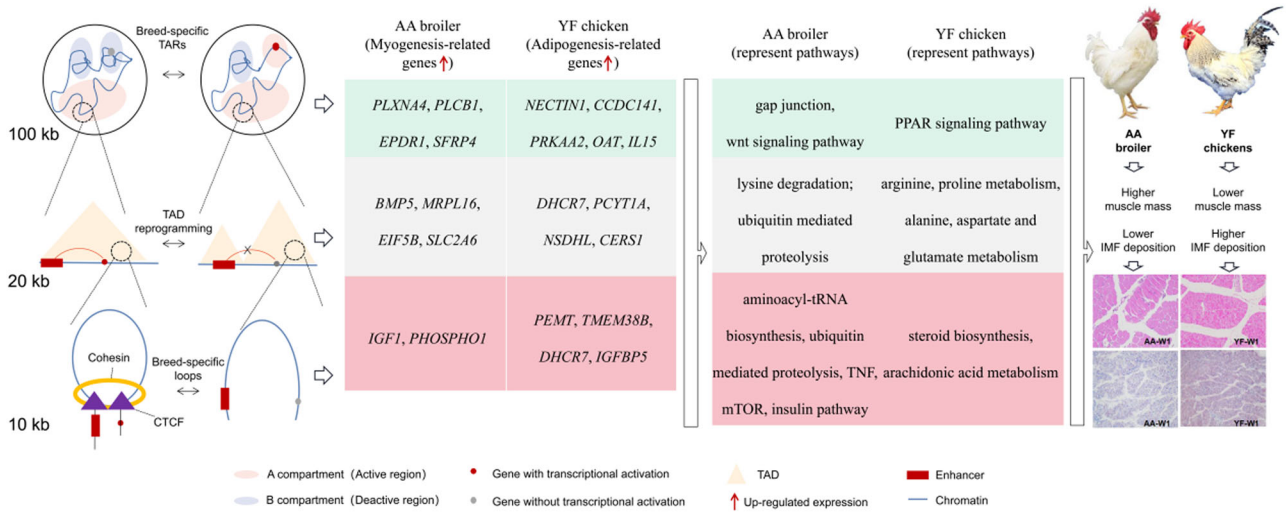

Fig. 7 | Proposed regulatory model for dynamic chromatin architecture on the transcriptional regulation of genes responsible for skeletal muscle growth and IMF deposition. The left track showed the 3D chromatin architecture in the level of compartment, TAD and loops from top to bottom; the second track showed the AA-specific or YF specific up-regulated genes regulated by compartment, TAD and loops from top to bottom; the third track showed Bup-DEGs represent pathways in the level of compartment, TAD and loops from top to bottom; the right track showed the difference in muscle fiber diameter and IMF deposition between AA broiler and YF chicken.

Animals and sampling

YF chickens and fertilized eggs were obtained from the Animal Center of Henan Agricultural University. AA broilers and fertilized eggs were obtained from a commercial AA broiler breeding farm. One hundred fertilized eggs of each breed were incubated in a humidified incubator with standard conditions (temperature 37.8 °C, humidity 55%, turned once per hour for the first 18 days; 37 °C and 75% humidity on days 19 and 20). Fifty embryos from each breed were harvested at E6 and E18 and male embryos were selected for sex identification[66]. The AA and YF chickens were raised according to the corresponding feeding standards, respectively. Ten male birds of each breed were euthanized at both D1 and W1. The left breast muscle of all individuals was extracted, snap-frozen in liquid nitrogen, then stored at -80 °C until use. The right breast muscle of all individuals was removed and placed in a 4% paraformaldehyde solution (Solarbio, Beijing, China) for histological experiments.

Hematoxylin-eosin (HE) staining and measurement of muscle fiber diameter

The fixed muscle tissues were embedded in paraffin and cut into 4 μm transverse sections. Sections were stained with hematoxylin and eosin. The 4 slides (n = 4) from per samples were observed using a light microscope (magnification, ×400). Five sites from each slide were randomly selected to measure the mean diameters of 100 myofibers and 50 myofiber bundles using DP2-BSW 2.2 software (Olympus, Tokyo, Japan).

Oil red O staining

Fixed tissue slices were embedded in an optimal cutting temperature compound (Sakura Finetek USA, Inc., Torrence, CA, USA) and cut into 10 μm sections using a freezing microtome. Three biological replicates were used for each breast muscle sample. 4% paraformaldehyde was used to fix frozen muscle sections for 15 min. Oil Red O working solution (Servicebio, Wuhan, China) was used to stain the tissue for 10 min in the dark and the slices were washed three times with water for 5 min each. After differentiation in 75% ethyl alcohol, the cell nuclei were quickly differentiated with hydrochloric acid alcohol, re-stained with hematoxylin for 5 min, and then dyed blue with an ammonia solution. Image Pro Plus 6.0 software (version 6.0; Media Cybernetics, Rockville, MD, USA) was used to normalize the lipid droplets areas. At the same time, each positive region were measured area in each photo. And the percentage of positive area (%) = the area of the lipid droplets/the area of the photo × 100.

Hi-C library construction, sequencing, and processing

Two biological replicates were prepared for each time point. In situ Hi-C analysis was performed on each sample as Rao et al [67]. Briefly, muscle tissues were crosslinked with 1 mL of freshly prepared 1% formaldehyde solution and incubated for 10 min at 35 °C. The reaction was quenched by adding glycine solution to a final concentration of 0.2 M. Tissues were lysed and chromatin was digested with 200 U of MboI restriction enzyme for 16 h at 37 °C. Digested DNA ends were labeled with biotinylated nucleotides and incubated at 37 °C for 90 min. Fragments were proximity ligated by adding T4 DNA ligase and incubated at 4 °C for 1 h, followed by 4 h at room temperature. Samples were supplemented with SDS, proteinase K, and NaCl to reverse crosslinking and incubated overnight at 65 °C. Subsequently, the DNA fragments were purified and sheared by sonication to generate DNA fragments in the 300–500 bp range. Ligation junctions labeled with biotin were pulled down using streptavidin C1 beads in preparation for BGI sequencing. Hi-C libraries were sequenced using an MGI-2000RS (BGI; Beijing, China). Hi-C experiments and library sequencing were performed by Frasergen Co., Ltd. (Wuhan, China). The original data from this platform were stored in FASTQ files. After quality controlling and filtering (Trimmomatic, v0.40)[68], the clean paired-end reads were aligned to the chicken reference genome (GRCg6a; ftp://ftp.ensembl.org/pub/release-104/fasta/gallus_gallus/dna) via Bowtie2 (v 2.2.8) recruited by ICE. After unmapped, single-side, dangling ends, and self-circle reads were removed, valid pairs in 200, 100, 20, and 10 kb bins were normalized to construct genomic interaction matrices of varying precision using HiC-Pro software (v 2.0)[69]. HiCdat (vtR _0.99)[70] was used to calculate the relationship between the interaction frequency and genomic linear distance. The R (v 4.0.0) was used to perform Pearson correlation coefficient analysis at a 200 kb resolution. In addition, the libraries YF_E6_2, YF_E18_1, YF_E18_2, YF_D1_1 and YF_D1_2 exhibit lower quality with lower *cis*-interaction percentage.

A/B compartment analysis

A PC1 vector of each sample Chr was produced using principal component analysis at a resolution of 100 kb and the Spearman correlation between the PC1 and genomic characteristics (gene density, GC content, and expression level) was computed. Compartment A corresponded to bins with a positive Spearman value, and compartment B corresponded to the rest of the genome. Next, to detect the switched compartment, the compartment types (A or B) across four periods were calculated. If the compartment type remained consistent across four periods, it was inferred that this compartment did not switch during muscle development. If there was a period during muscle development where the compartment type differed from the other three periods, it was considered that a compartment switching event occurred during muscle development. Furthermore, the TARs and breed-specific TARs according to the switched compartment were analyzed. In detail, TARs were the genome showed stable A-to-A compartments and switched B-to-A compartments from former to later stages. The breed-specific TARs indicate the switched compartments between adjacent stages were only detected in a certain breed. For example, AA-specific TARs from E6 to E18 were A-to-A/B-to-A compartment in AA broilers, but showed B-to-B/A-to-B compartment in YF chickens. Similarly, YF-specific TARs from E6 to E18 were A-to-A/B-to-A compartment in YF chickens, but showed B-to-B/A-to-B compartment in AA broilers.

TAD analysis

TADs were called using cworld-dekker (https://github.com/dekkerlab/cworld-dekker) at the best resolution for each Chr. This algorithm is commonly used for calling TADs in plants[8] and animals[71]. In detail, we calculated IS (insulation score) using matrix2insulation.pl (version 1.0.0) with the parameters (—v -is 200,000 -ids 80,000 -im mean -nt 0.1 -bmoe 0) at 20-kb resolution. The IS of each 20-kb bin was determined by calculating the average number of interactions across the bins. The interquartile range (IQR) mean signal of a 20 kb bin was calculated based on the values of interactions and assigned to the diagonal bin with a size of 20 kb. Then, we performed this process on all bins. The IS was normalized relative to all of the IS across each chromosome by calculating the log2 ratio of each bin's IS versus the mean of all IS. The minimum values along the normalized IS vector were interpreted as TAD boundaries or regions with high local insulation.

Based on the TADs calculated by IS, we performed pairwise TAD reprogramming analysis. We called the bedtools to calculate the proportion of overlapping TADs between two adjacent stages according to Renschler et al [72]. Berifly, we employed "intersect" parameter to count the proportion of overlapping TADs in paired TADs. Then, we divided TAD reprogramming into stable TADs exhibited alternation of intra-interaction frequency or sliding TAD exhibited different boundaries between adjacent periods. We compared all TADs of one sample with all TADs of another sample. If the overlapped proportion of the TAD in two adjacent stages was above 0.75, the TAD between these two stages was considered stable. Otherwise, if two or more TADs in priod stage responded to one TAD in later stage, this change was called 'merge'; if one TAD in priod stage responded to 2 or more TADs in later stage, this change was called 'split'. Expected to the TAD 'merge' and 'split', the remaining states were defined as TAD rearrangement[73]. Therefore, we obtained one-to-many (split), many-to-one (merge), or other corresponding relationships (rearrangement) between TADs in adjacent periods, and can further count and quantify the merged, split and rearranged TADs during adjacent stages. In addition, the D-score was used to quantify intra-TAD interactions[74] in stable TADs. For each TAD, we calculated the D-score as the fraction of intraTAD contacts over

the total number of intrachromosomal contacts for a TAD (intraTAD + interTAD). Intra-TAD interaction differences between adjacent physiological periods were analyzed by normalizing the TAD of samples from adjacent periods by the diff.matrix[24].

Significant chromosome interactions identification

We used the FitHIC (v2.0.7) (https://github.com/ay-lab/fithic) to identify chromatin loops at a matrix resolution of 10 kb[75]. Only interactions where $p \le 0.01$, $q \le 0.01$ and the number of reads mapping the interaction was >2 were judged to be significant interactions.

To compare the differential loops during muscle development between two breeds, we firstly defined three types of loops during adjacent stages, including emerging loops referring to loops formed during the later of the adjacent periods, missing loops referring to loops formed in an earlier period but disappeared in the later adjacent periods, unchanging loops referring to loops that appear in both adjacent periods.

Then, we calculated the similarity rate of different loop types was calculated as follows: common loops in paired adjacent periods between two breeds/(the loops of AA broiler + the loops of YF chicken) in paired adjacent periods. For example, the similarity rate of emerging loops from D1 to W1 was calculated, resulting in a total count of 41,692 loops defined as emerging loops in both AA and YF chicken. Meanwhile, there were a total of 292,233 loops from D1 to W1 in both two breeds, so the similarity rate of emerging loops from D1 to W1 was 41692/292233 = 0.1426 (14.26%, the data came from supplementary Data 4). By employing this concept, we computed the similarity rates of various loop types across four developmental stages and evaluated the disparities in dynamic loops between two breeds. Heatmaps were used for the visual inspection of local chromatin interaction frequency changes based on the differential matrix of loops derived from the average number of z-score differences between adjacent periods of 10 kb bins[25]. To analyze the difference in loop interactions between different stages, the loop track and differential matrix between different samples were compared, such as *PEMT*. If the differentiation of loop interactions cannot be identified by the aforementioned two tracks, the diff.matrix value was utilized to address this issue, such as *IGFBP5*.

ATAC-seq

Breast muscle samples were the same as those used for Hi-C library preparation. Muscle nucleus suspensions were incubated in a transposition mix containing transposase. The transposition reaction was performed at 37 °C for 30 min, then the DNA was purified from the reaction mixture using a QIAGEN minielute kit (Qiagen; MD, USA)[76]. Samples were sequenced using an llumina NovaSeq 6000 system (Illumina; San Diego, CA, USA) and data were stored as FASTQ files.

ATAC-seq data processing

Raw reads with adapters, reads with more than 10% of unknown nucleotides (N), and reads of low quality (q-value ≤ 20) were removed to get high quality clean reads via Bowtie2[77] (v 2.2.8). Clean reads were aligned to the reference genome (GRCg6a). All concordantly aligned paired mates were used for peak calling in MACS[78] (v. 2.1.2). A dynamic Poisson distribution was used to calculate the p-value of a specific region based on unique mapped reads. A region was defined as a peak when $q < 0.05$. Peak-related genes were confirmed according to gene annotation and the genomic location of the peak using ChIPseeker[79] (v 1.16.1). The distribution of peaks on different genome regions (promoter, 5'UTR, 3'UTR, exon, intron, downstream, and intergenic regions) were analyzed. The conserved DNA motifs for TFs binding through the peak regions were scanned using MEME-ChIP and the existence of any known motifs was confirmed using MEME-AME[80].

To compare the accessibility of chromatin the following steps were performed: (1) The peaks detected in each sample were combined to obtain the total set of peaks. (2) The position in the set, background value, and signal value (FPKM) of each peak were extracted for each sample and the signal value was divided by the background value to obtain the enrichment fold of the peak. (3) The DAR between groups was analyzed using DESeq2 software[81] (v 3.16) with the filtering threshold was set to |log2 (fold change)| >2 and p-value < 0.05 to obtain the DAR between sample groups.

RNA extraction and RNA-seq library preparation

The sampling protocol was the same as that for the Hi-C and ATAC-seq library construction with an additional biological replicate. Total RNA was extracted from the tissues using TRIzol reagent (Takara Bio Inc.; Kyoto, Japan) according to the manufacturer's protocol. The RNA integrity was determined by 1.5% denaturing agarose gel electrophoresis, and the RNA purity and concentration were measured using a NanoDrop2000 (Thermo Scientific; Wilmington, DE, USA). Sequencing libraries were generated using the rRNA-depleted RNA by NEBNext® Ultra™ Directional RNA Library Prep Kit for Illumina® (NEB; Beijing, China) following the manufacturer's protocol. RNA-seq libraries were sequenced using an MGI-2000RS (BGI). Clean reads were obtained using the same filtering conditions as ATAC-seq data processing.

RNA-seq data analysis

Clean reads were aligned to GRCg6a using HISAT2 (v 2.2.1)[82]. The output files were imported into StringTie[83] to assemble and quantify transcriptomes. The output GTF files containing the assembled transcripts and expression abundance of genes in each library were normalized using FPKM. Three biological replicates were used. Differential expression analyses between groups were performed using DESeq2[81]. DEGs were deemed significant if they passed the following cutoff parameters: absolute value of log2 fold change >1 and q-value < 0.05.

GO enrichment analysis

All concerned genes were mapped to GO terms in the Gene Ontology database (http://www.geneontology.org/), gene numbers were calculated for every term, and significantly enriched GO terms in concerned genes compared to the genome background were defined by a hypergeometric test. P-values calculated using hypergeometric tests were corrected to q-values. When $q < 0.05$, GO terms were defined as significantly enriched for the concerned gene.

KEGG enrichment analysis

All concerned genes were mapped to pathways in the Kyoto Encyclopedia of Genes and Genomes (KEGG) databases. The significantly enriched pathways of concerned genes compared to the chicken genome (GRCg6a) were defined by a over-represented test. The p-values calculated using hypergeometric tests were adjusted for multiple testing to obtain q-values. The significance level of $q < 0.05$ was adopted as the threshold standard.

TF identification

The amino acid sequences of genes were used as input files for the prediction of TFs using AnimalTFDB 3.0 (http://bioinfo.life.hust.edu.cn/AnimalTFDB/#!/predict)[84]. If $p < 0.01$, the TFs were identified as plausible.

Statistics and reproducibility

A completely random design was used for sampling according to random numbers. The number of samples per breeds ranged from 10-15 for Hi-C, ATAC and RNA-seq. Integrated analysis requires retrieval of Bup-DEGs and ATAC-peaks on the 10 kb loop anchor. When genes or peaks overlapped with the loop anchor by more than 75%, these genes and peaks were located on this loop anchor. A list of the code/software described in the paper and parameters used when running the software can be found at this link[85]. Each replicate served as the experimental unit for all statistical analyses. Data are presented as means ± standard deviations (SD). Statistical analysis was performed using Minitab 20.2.0 Software (Minitab LLC; State College, PA, USA). Student's t-test was used with two-tailed distribution and two-sample equal variance. For each t-test, the degrees of freedom were recorded were shown in the corresponding figure legends. For each Wilcoxon rank-sum tests, the sample numbers were shown in the

corresponding figures or supplementary data. A p-value < 0.05 was considered to be statistically significant difference. All general information on study design, statistical analysis of data and reproducibility of experiments were stated in related figure/table, figure legends and supplementary data.

Reporting summary

Further information on research design is available in the Nature Portfolio Reporting Summary linked to this article.

Data availability

The Hi-C raw data of breast muscle generated in this study were deposited in China National Center for Bioinformation Genome Sequence Archive (CNCB-GSA) with accession number PRJCA025668 (https://ngdc.cncb.ac.cn/gsa/browse/CRA016298). The ATAC-seq raw data of breast muscle generated in this study were deposited in NCBI Sequence Read Archive (NCBI-SRA) with accession number PRJNA962614. The RNA-seq raw data of breast muscle generated in this study were deposited in NCBI-SRA with accession number PRJNA729271. The above raw data was used to generate Fig. 1b; Fig. 2a, d, e; Fig. 3 f, g; Fig. 6 c, d; Supplementary Fig. 2; Supplementary Fig. 3a, c-d; Supplementary Fig. 5a, d-h; Supplementary Fig. 6 b-d, j-i; Supplementary Fig. 7; Supplementary Fig. 8c, d-e; Supplementary Fig. 9c; Supplementary Fig. 10; and five Supplementary tables. The Supplementary data 1 contain the source data of Fig. 2b. The Supplementary data 2 contain the source data of Fig. 2c, Supplementary Fig. 1 b,d; and Supplementary Fig. 5b,c. The Supplementary data 3 contain the source data of Fig. 3 a, b, e; Supplementary Fig. 6 a, e-f. The Supplementary data 4 contain the statistical value of Fig. 4a, and the loops can be detected from the raw data of Hi-C. The Supplementary data 5 contain the source data of Fig. 5 a–c, Supplementary Fig. 3b and Supplementary Fig. 8a. The Supplementary data 6 and 7 contain the source data of Fig. 6b and Supplementary Fig. 9a-b. Supplementary Data 8 contain the source data of Fig. 3b, c. Supplementary Data 9 contain the source data of Fig. 4b. Supplementary Data 10 contain the source data of Fig. 6b. All other data are available from the corresponding author (or other sources, as applicable) on reasonable request.

Received: 15 October 2023; Accepted: 17 July 2024;
Published online: 28 July 2024

References

1. El-Senousey, H. K., Fouad, A. M., Yao, J. H., Zhang, Z. G. & Shen, Q. W. Dietary alpha lipoic Acid improves body composition, meat quality and decreases collagen content in muscle of broiler chickens. *Asian-Australas. J. Anim. Sci.* **26**, 394–400 (2013).
2. Picard, B., Lefaucheur, L., Berri, C. & Duclos, M. J. Muscle fibre ontogenesis in farm animal species. *Reprod. Nutr. Dev.* **42**, 415–431 (2002).
3. Velleman, S. G. Relationship of Skeletal Muscle Development and Growth to Breast Muscle Myopathies: A Review. *Avian Dis.* **59**, 525–531 (2015).
4. Scaal, M. & Marcelle, C. Chick muscle development. *Int. J. Dev. Biol.* **62**, 127–136 (2018).
5. Yan, X., Zhu, M. J., Dodson, M. V. & Du, M. Developmental programming of fetal skeletal muscle and adipose tissue development. *J. Genom.* **1**, 29–38 (2013).
6. Zhang, Y. et al. Transcriptome analysis of the pectoral muscles of local chickens and commercial broilers using Ribo-Zero ribonucleic acid sequencing. *PLoS One* **12**, e0184115 (2017).
7. Chen, C. et al. A global view of porcine transcriptome in three tissues from a full-sib pair with extreme phenotypes in growth and fat deposition by paired-end RNA sequencing. *BMC Genom.* **12**, 448 (2011).
8. Zhang, X. et al. Chromatin spatial organization of wild type and mutant peanuts reveals high-resolution genomic architecture and interaction alterations. *Genome Biol.* **22**, 315 (2021).
9. Van, A., Huylebroeck, D., Hendriks, R. W. & Stadhouders, R. 3D genome organization during lymphocyte development and activation. *Brief. Funct. Genom.* **19**, 71–82 (2020).
10. Cremer, M. & Brandstetter, K. Cohesin depleted cells rebuild functional nuclear compartments after endomitosis. *Nat. Commun.* **11**, 6146 (2020).
11. Dixon, J. R. et al. Chromatin architecture reorganization during stem cell differentiation. *Nature* **518**, 331–336 (2015).
12. Dowen, J. M. et al. Control of cell identity genes occurs in insulated neighborhoods in mammalian chromosomes. *Cell* **159**, 374–387 (2014).
13. Hnisz, D. et al. Activation of proto-oncogenes by disruption of chromosome neighborhoods. *Science* **351**, 1454–1458 (2016).
14. Lupiáñez, D. G. et al. Disruptions of topological chromatin domains cause pathogenic rewiring of gene-enhancer interactions. *Cell* **161**, 1012–1025 (2015).
15. Nora, E. P. et al. Targeted degradation of CTCF decouples local insulation of chromosome domains from genomic compartmentalization. *Cell* **169**, 930–944 (2017).
16. Wutz, G. et al. Topologically associating domains and chromatin loops depend on cohesin and are regulated by CTCF, WAPL and PDS5 proteins. *EMBO J.* **36**, 3573–3599 (2017).
17. Flavahan, W. A. et al. Insulator dysfunction and oncogene activation in IDH mutant gliomas. *Nature* **529**, 110–114 (2016).
18. Franke, M. et al. Formation of new chromatin domains determines pathogenicity of genomic duplications. *Nature* **538**, 265–269 (2016).
19. Grubert, F. et al. Landscape of cohesin-mediated chromatin loops in the human genome. *Nature* **583**, 737–743 (2020).
20. Hao, R. H. & Guo, Y. Lineage-specific rearrangement of chromatin loops and epigenomic features during adipocytes and osteoblasts commitment. *Cell Death Differ.* **29**, 2503–2518 (2022).
21. Buenrostro, J. D., Giresi, P. G., Zaba, L. C., Chang, H. Y. & Greenleaf, W. J. Transposition of native chromatin for fast and sensitive epigenomic profiling of open chromatin, DNA-binding proteins and nucleosome position. *Nat. Methods* **10**, 1213–1218 (2013).
22. Li, J. et al. Enhancer-promoter interaction maps provide insights into skeletal muscle-related traits in pig genome. *BMC Biol.* **20**, 136 (2022).
23. Wang, R., Chen, F., Chen, Q. & Wan, X. MyoD is a 3D genome structure organizer for muscle cell identity. *Nat. Commun.* **13**, 205 (2022).
24. Li, D., Ning, C., Zhang, J. & Wang, Y. Dynamic transcriptome and chromatin architecture in granulosa cells during chicken folliculogenesis. *Nat. Commun.* **13**, 131 (2022).
25. Fishman, V. et al. 3D organization of chicken genome demonstrates evolutionary conservation of topologically associated domains and highlights unique architecture of erythrocytes' chromatin. *Nucleic Acids Res* **47**, 648–665 (2019).
26. Tian, W. et al. Chromatin interaction responds to breast muscle development and intramuscular fat deposition between chinese indigenous chicken and fast-growing broiler. *Front. Cell Dev. Biol.* **9**, 782268 (2021).
27. Lieberman-Aiden, E. et al. Comprehensive mapping of long-range interactions reveals folding principles of the human genome. *Science* **326**, 289–293 (2009).
28. Englmaierová, M., Skřivan, M., Taubner, T., Skřivanová, V. & Čermák, L. Effect of housing system and feed restriction on meat quality of medium-growing chickens. *Poult. Sci.* **100**, 101223 (2021).
29. Velleman, S. G. Recent developments in breast muscle myopathies associated with growth in poultry. *Annu. Rev. Anim. Biosci.* **7**, 289–308 (2019).
30. Hosotani, M. et al. The unique physiological features of the broiler pectoralis major muscle as suggested by the three-dimensional ultrastructural study of mitochondria in type IIb muscle fibers. *J. Vet. Med. Sci.* **83**, 1764–1771 (2021).

31. Southard, S., Kim, J. R., Low, S., Tsika, R. W. & Lepper, C. Myofiber-specific TEAD1 overexpression drives satellite cell hyperplasia and counters pathological effects of dystrophin deficiency. *Elife* **5**, e15461 (2016).
32. Taniura, H., Kuo, C. H., Hayashi, Y. & Miki, N. Purification and characterization of an 82-kD membrane protein as a neurite outgrowth factor binding protein: possible involvement of NOF binding protein in axonal outgrowth in developing retina. *J. Cell Biol.* **112**, 313–322 (1991).
33. Schmidt, F. et al. The E3 ubiquitin ligase TRIM62 and inflammation-induced skeletal muscle atrophy. *Crit. Care* **18**, 545 (2014).
34. Meng, L. et al. Specific lysophosphatidylcholine and acylcarnitine related to sarcopenia and its components in older men. *BMC Geriatr.* **22**, 249 (2022).
35. He, M. et al. Genome-wide chromatin structure changes during adipogenesis and myogenesis. *Int. J. Biol. Sci.* **14**, 1571–1585 (2018).
36. Rahbek, S. K. et al. Effects of divergent resistance exercise contraction mode and dietary supplementation type on anabolic signalling, muscle protein synthesis and muscle hypertrophy. *Amino Acids* **46**, 2377–2392 (2014).
37. Ingwall, J. S. et al. Creatine: a possible stimulus skeletal cardiac muscle hypertrophy. *Recent Adv. Stud. Card. Struct. Metab.* **8**, 467–481 (1975).
38. Sarsenbek, A., Wang, T., Zhao, J. K. & Jiang, W. Comparison of carcass yields and meat quality between Baicheng-You chickens and Arbor Acres broilers. *Poult. Sci.* **92**, 2776–2782 (2013).
39. Huang, Z. et al. Analysis of the molecular mechanism of inosine monophosphate deposition in Jingyuan chicken muscles using a proteomic approach. *Poult. Sci.* **4**, 101741 (2022).
40. Qiu, Y. Y. et al. Mitochondrial dysfunction resulting from the down-regulation of bone morphogenetic protein 5 may cause microtia. *Ann. Transl. Med.* **9**, 418 (2021).
41. Smith, K., Reynolds, N., Downie, S., Patel, A. & Rennie, M. J. Effects of flooding amino acids on incorporation of labeled amino acids into human muscle protein. *Am. J. Physiol.* **1**, E73–E78 (1998).
42. Mitchell, W. K. et al. Human Skeletal Muscle Protein Metabolism Responses to Amino Acid Nutrition. *Adv. Nutr.* **7**, 828S–838SS (2016).
43. Post, A. et al. Plasma creatine concentration is associated with incident hypertension in a cohort enriched for the presence of high urinary albumin concentration: the Prevention of Renal and Vascular Endstage Disease study. *J. Hypertens.* **40**, 229–239 (2022).
44. Ali, M. et al. Comparison of Functional Compounds and Micronutrients of Chicken Breast Meat by Breeds. *Food Sci. Anim. Resour.* **39**, 632–642 (2019).
45. Ulrich, R., Kalkuhl, A., Deschl, U. & Baumgärtner, W. Machine learning approach identifies new pathways associated with demyelination in a viral model of multiple sclerosis. *J. Cell. Mol. Med* **14**, 434–448 (2010).
46. Andreone, B. J. et al. Blood-brain barrier permeability is regulated by lipid transport-dependent suppression of caveolae-mediated transcytosis. *Neuron* **94**, 581–594 (2017).
47. Yuan, R. et al. Reorganization of chromatin architecture during prenatal development of porcine skeletal muscle. *DNA Res.* **28**, dsab003 (2021).
48. Cheng, N., Li, G., Kanchwala, M. & Evers, B. M. STAG2 promotes the myelination transcriptional program in oligodendrocytes. *Elife* **11**, e.77848 (2022).
49. Zhan, Y. et al. Reciprocal insulation analysis of Hi-C data shows that TADs represent a functionally but not structurally privileged scale in the hierarchical folding of chromosomes. *Genome Res* **27**, 479–490 (2017).
50. Du, Y. & Gu, Z. Dynamic interplay between structural variations and 3D genome organization in pancreatic cancer. *Adv. Sci.* **9**, e2200818 (2022).
51. Lebaron, S. et al. Proofreading of pre-40S ribosome maturation by a translation initiation factor and 60S subunits. *Nat. Struct. Mol. Biol.* **19**, 744–753 (2012).
52. Jiang, X. et al. Slc2a6 regulates myoblast differentiation by targeting LDHB. *Cell Commun. Signal.* **20**, 107 (2022).
53. Caldas, H. & Herman, G. E. NSDHL, an enzyme involved in cholesterol biosynthesis, traffics through the Golgi and accumulates on ER membranes and on the surface of lipid droplets. *Hum. Mol. Genet.* **12**, 2981–2991 (2003).
54. Bouchoux, J. et al. The proteome of cytosolic lipid droplets isolated from differentiated Caco-2/TC7 enterocytes reveals cell-specific characteristics. *Biol. Cell* **103**, 499–517 (2011).
55. Turner, N., Lim, X. Y. & Toop, H. D. A selective inhibitor of ceramide synthase 1 reveals a novel role in fat metabolism. *Nat. Commun.* **9**, 3165 (2018).
56. Kaiser, V. B. & Semple, C. A. Chromatin loop anchors are associated with genome instability in cancer and recombination hotspots in the germline. *Genome Biol.* **19**, 101 (2018).
57. Gibcus, J. H. & Dekker, J. The hierarchy of the 3D genome. *Mol. Cell* **49**, 773–782 (2013).
58. West, A. G. & Fraser, P. Remote control of gene transcription. *Hum. Mol. Genet.* **14**, R101–R111 (2005).
59. Hintermann, A. et al. Developmental and evolutionary comparative analysis of a regulatory landscape in mouse and chicken. *Development* **149**, dev200594 (2022).
60. Pan, Z. et al. An atlas of regulatory elements in chicken: A resource for chicken genetics and genomics. *Sci. Adv.* **9**, eade1204 (2023).
61. Chal, J. & Pourquié, O. Making muscle: skeletal myogenesis in vivo and in vitro. *Development* **144**, 2104–2122 (2017).
62. Goodfellow, F. T. et al. Zika virus induced mortality and microcephaly in chicken embryos. *Stem Cells Dev.* **25**, 1691–1697 (2016).
63. Zanou, N. & Gailly, P. Skeletal muscle hypertrophy and regeneration: interplay between the myogenic regulatory factors (MRFs) and insulin-like growth factors (IGFs) pathways. *Cell. Mol. Life. Sci.* **70**, 4117–4130 (2013).
64. Marsman, J., Gimenez, G., Day, R. C., Horsfield, J. A. & Jones, G. T. A non-coding genetic variant associated with abdominal aortic aneurysm alters ERG gene regulation. *Hum. Mol. Genet.* **29**, 554–565 (2020).
65. Zhao, L. et al. Chromatin loops associated with active genes and heterochromatin shape rice genome architecture for transcriptional regulation. *Nat. Commun.* **10**, 3640 (2019).
66. Bantock, T. M., Prys-Jones, R. P. & Lee, P. L. New and improved molecular sexing methods for museum bird specimens. *Mol. Ecol. Resour.* **8**, 519–528 (2008).
67. Rao, S. S. et al. A 3D map of the human genome at kilobase resolution reveals principles of chromatin looping. *Cell* **159**, 1665–1680 (2014).
68. Bolger, A. M., Lohse, M. & Usadel, B. Trimmomatic: a flexible trimmer for Illumina sequence data. *Bioinformatics* **30**, 2114–2120 (2014).
69. Servant, N. et al. HiC-Pro: an optimized and flexible pipeline for Hi-C data processing. *Genome Biol.* **16**, 259 (2015).
70. Schmid, M. W., Grob, S. & Grossniklaus, U. HiCdat: a fast and easy-to-use Hi-C data analysis tool. *BMC Bioinforma.* **16**, 277 (2015).
71. Ke, Y. et al. 3D Chromatin Structures of Mature Gametes and Structural Reprogramming during Mammalian Embryogenesis. *Cell* **170**, 367–381.e320 (2017).
72. Renschler, G. & Richard, G. Hi-C guided assemblies reveal conserved regulatory topologies on X and autosomes despite extensive genome shuffling. *Genes Dev.* **33**, 1591–1612 (2019).
73. Crane, E. et al. Condensin-driven remodelling of X chromosome topology during dosage compensation. *Nature* **523**, 240–244 (2015).
74. Krijger, P. H. et al. Cell-of-origin-specific 3D genome structure acquired during somatic cell reprogramming. *Cell Stem Cell* **18**, 597–610 (2016).
75. Kaul, A. & Bhattacharyya, S. Identifying statistically significant chromatin contacts from Hi-C data with FitHiC2. *Nat. Protoc.* **15**, 991–1012 (2020).

76. Zhu, X. N. et al. Chicken chromatin accessibility atlas accelerates epigenetic annotation of birds and gene fine-mapping associated with growth traits. *Zool. Res.* **44**, 53–62 (2023).
77. Langmead, B. & Salzberg, S. L. Fast gapped-read alignment with Bowtie 2. *Nat. Methods* **9**, 357–359 (2012).
78. Zhang, Y. et al. Model-based analysis of ChIP-Seq (MACS). *Genome Biol.* **9**, R137 (2008).
79. Yu, G., Wang, L. G. & He, Q. Y. ChIPseeker: an R/bioconductor package for ChIP peak annotation, comparison and visualization. *Bioinformatics* **31**, 2382–2383 (2015).
80. Bailey, T. L. et al. MEME SUITE: tools for motif discovery and searching. *Nucleic Acids Res* **37**, W202–W208 (2009).
81. Love, M. I., Huber, W. & Anders, S. Moderated estimation of fold change and dispersion for RNA-seq data with DESeq2. *Genome Biol.* **15**, 550 (2014).
82. Kim, D., Langmead, B. & Salzberg, S. L. HISAT: a fast spliced aligner with low memory requirements. *Nat. Methods* **12**, 357–360 (2015).
83. Pertea, M. et al. StringTie enables improved reconstruction of a transcriptome from RNA-seq reads. *Nat. Biotechnol.* **33**, 290–295 (2015).
84. Hu, H. et al. AnimalTFDB 3.0: a comprehensive resource for annotation and prediction of animal transcription factors. *Nucleic Acids Res* **47**, D33–D38 (2019).
85. Zenodo Repository. https://doi.org/10.5281/zenodo.11091365.

Acknowledgements

This study was supported by the Natural Science Foundation of China (32172720), National Key Research and Development Program (2022YFF1000202), and Major Scientific and Technological Special Project of Henan Province (NO.221100110200).

Author contributions

Z.W. performed the majority of conceptualization and the analytical strategy. Z.W., W.T., and Y.G. performed statistical analysis and drafted the manuscript. D.W., Z.Y. and Y.Z. help to hatch and feed the experimental animals. D.L., W.L., and Z.L. collect the samples. R.J., R.H., G.S., G.L., and Y.T. designed and performed bioinformatics analysis. H.L. participated in the design of the study and helped to revise the manuscript. X.K. and X.L. designed and provided overall supervision. All authors read and approved the final manuscript.

Competing interests

The authors declare no competing interests.

Additional information

Supplementary information The online version contains supplementary material available at https://doi.org/10.1038/s42003-024-06599-3.

Correspondence and requests for materials should be addressed to Hong Li, Xiangtao Kang or Xiaojun Liu.

Peer review information *Communications Biology* thanks Anne-Laure Valton, Tatsuhiko Goto, and Alla Krasikova for their contribution to the peer review of this work. Primary Handling Editors: Eirini Trompouki and David Favero. A peer review file is available.